Eur. Phys. J. D **10**, 53–65 (2000)

THE EUROPEAN PHYSICAL JOURNAL D

EDP Sciences

Near threshold photoionization of excited alkali atoms Ak(np) (Ak = Na, K, Rb, Cs; n = 3–6)

I.D. Petrov[1,2], V.L. Sukhorukov[1,2], E. Leber[1], and H. Hotop[1,a]

[1] Fachbereich Physik, Universität Kaiserslautern, 67653 Kaiserslautern, Germany
[2] Rostov State University of Transport Communications, 344038 Rostov-on-Don, Russia

Received 21 July 1999 and Received in final form 14 October 1999

Abstract. The effect of the polarization of the atomic core by the outer electron on near threshold photoionization of excited alkali atoms Ak(np) (Ak = Na–Cs; $n = 3-6$) is investigated. Partial and total cross-sections for photo-ionization of the np-electron were computed utilizing the configuration interaction technique with Pauli-Fock atomic orbitals (CIPF) and including the long range core polarization potential (CP). To calculate the core polarization potential the variational principle is applied. Comparison with previous theoretical results and with available experimental data is made for the total cross-section σ, for the electron angular distribution parameter β, for the ratio $\nu = |D_{\rm d}/D_{\rm s}|$ of the reduced electric dipole matrix elements and for the phase shift difference $\Delta = \delta_{\rm d} - \delta_{\rm s}$, associated with the d-wave and s-wave continua, respectively. In the comparison, new experimental results for σ, ν, and Δ, measured for laser-excited, polarized ^{39}K($4p_{3/2}$) atoms, have been included.

PACS. 32.80.Fb Photoionization of atoms and ions – 33.60.-q Photoelectron spectra – 31.50.+w Excited states

1 Introduction

Photoionization of excited atoms is an important elementary process in applied plasmas such as discharges, laser media and flames. In spite of its relevance, rather few quantitative studies have so far been carried out of the respective energy dependent near-threshold cross-sections; determinations of partial, final-state cross-sections or of the relevant basic quantities (electric dipole elements and phase shifts of the photoelectron continuum waves) are scarce for excited states [1,2]. Alkali atoms as quasi-one-electron systems have proven to be an important and interesting testing ground for theoretical descriptions of the photoionization process, both for *ab initio* theories and semiempirical calculations. In particular, photoionization of alkali atoms in their ground state Ak(ns) has received a lot of attention due to the Cooper-Seaton minimum appearing close to threshold for Ak = Na, K, Rb, and Cs ($n = 3-6$) which provides a sensitive probe of electron correlation and relativistic effects [3,4]. In a recent paper, we have described a novel approach to include in these calculations the polarization of the core electrons by the outer valence electron in a realistic and efficient way [4]. For ground state alkali atoms, these core polarization effects have been known to be important for some time [5–12]. For outer electrons with less core-penetrating character it is expected that the effects of core polarization on near-threshold photoionization cross-sections are less important. In a recent study of photoionization of laser-excited K($4p_{3/2}$) atoms, carried out in connection with the development of an intense laser photoelectron source [13,14], we were quite surprised to observe strong deviations of our measured cross-sections from theoretical predictions based on the Hartree Fock approach which had been shown to provide good results for photoionization of excited Na($3p$) atoms [15].

These observations motivated us to carry out a systematic theoretical investigation of near-threshold photoionization of the excited Ak(np) states ($n = 3-6$) for Ak = Na, K, Rb and Cs:

$$\mathrm{Ak}(np) + \gamma \rightarrow \mathrm{Ak}^+ + e^-(\varepsilon s, \varepsilon d), \qquad (1)$$

where ε denotes the energy of the photoelectron. We use the configuration interaction Pauli Fock (CIPF) method, developed in previous work [2,16–20]. In order to account for core polarization effects we use an approach described in a recent paper and there applied to photoionization of ground state alkali atoms [4]. We report theoretical results for the total photoionization cross-sections $\sigma(\varepsilon)$, for the electron angular distribution of unpolarized excited atoms (characterized by the anisotropy parameter $\beta(\varepsilon)$), for the ratio $\nu(\varepsilon) = |D_{\rm d}/D_{\rm s}|$ of the electric dipole matrix elements and for the phase shift difference $\Delta(\varepsilon) = \delta_{\rm d} - \delta_{\rm s}$ associated with the d-wave and s-wave continua, respectively, at photoelectron energies from threshold up to 6 eV.

[a] e-mail: hotop@physik.uni-kl.de

The theoretical results are compared with existing literature data including recent experiments with cold, trapped Rb and Cs atoms as well as our new measurements for K($4p_{3/2}$) atoms. Differences between theory and experiment are critically discussed.

The paper is organized as follows: in Section 2 we describe the theoretical method. In Section 3 we sketch the experimental approach used to obtain our data for the excited K($4p_{3/2}$) atoms. In Section 4 we present the calculated results and compare them with previous theoretical and the experimental data.

2 Theory

2.1 Transition amplitude and cross-section

In order to calculate photoionization of excited alkali atoms Ak($n_0\ell_0 = 1, J_0$) we used the following scheme (written for the case of K($4p$) in (2)).

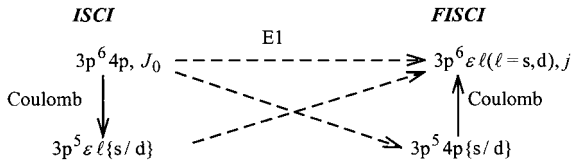

(2)

In this scheme we have included the configurations which contribute to the transition amplitude due to initial state configuration interaction (ISCI) and final state configuration interaction (FISCI). The solid and broken lines represent the Coulomb and electric dipole interaction E1, respectively; $\{\ell\}$ means a complete set of intermediate AOs, over which summation and integration are carried out.

The first horizontal line in scheme (2) represents the direct transition whereas the other lines are the many-electron corrections of the first order known as intershell correlations. Accounting for these intershell correlations in the considered problem somewhat increases the photoionization cross-sections and brings the results computed in length and velocity gauges into closer agreement, as will be illustrated in Section 2.3, Figure 2 and Table 1. The expression for the reduced matrix element of a direct transition in (2) can be simplified in comparison with that obtained in [19] because of the closed $3p$-shell and has the following form:

$$\langle \varepsilon\ell j||Q^{(1)}||n_0\ell_0 J_0\rangle = (-1)^{\ell+1/2+J_0+1}[(2j+1)(2J_0+1)]^{1/2} \times \begin{Bmatrix} \ell & j & 1/2 \\ J_0 & \ell_0 & 1 \end{Bmatrix} \langle \ell||C^{(1)}||\ell_0\rangle \langle \varepsilon\ell|d|n_0\ell_0\rangle \quad (3)$$

where the $6j$-symbol is defined according to [21].

In equation (3) $\langle \ell||C^{(1)}||\ell_0\rangle = \sqrt{\ell_{\max}}$ ($\ell_{\max} = \max(\ell, \ell_0)$) is the submatrix element of the spherical functions determined according to the standard phase convention [21] and is always positive, $\langle \varepsilon\ell|d|n_0\ell_0\rangle = \int_0^\infty P(\varepsilon\ell|r)dP(n_0\ell_0|r)\mathrm{d}r$ is the radial integral determined either in length ($d = r$) or velocity form ($d = (\mathrm{d}/\mathrm{d}r \mp \ell_{\max}/r)$ and the signs $-$ or $+$ corresponds to the transitions $\ell \to \ell - 1$, $\ell \to \ell + 1$). The formulae for the matrix elements of the correlation transitions in (2) are expressed *via* a sum of products of radial integrals of the dipole transition and Slater integrals. They have a rather bulky expression in general form and are not listed here. All these matrix elements including the direct amplitude written out in (3) depend on the quantum numbers j, ℓ and J_0. The expression for the total photoionization cross-section *via* the partial cross-sections $\sigma^{\ell j}_{J_0}(\omega)$ has the form:

$$\sigma_{J_0}(\omega) = \sum_{\ell j} \sigma^{\ell j}_{J_0}(\omega) \quad (4)$$

where $\sigma^{\ell j}_{J_0}(\omega)$ are determined according to the following formula:

$$\sigma^{\ell j}_{J_0}(\omega)[\mathrm{Mb}] = \frac{4}{3}\pi^2\alpha a_0^2\omega^{\pm 1}\frac{1}{2J_0+1}|\langle \varepsilon\ell j||D||J_0\rangle|^2. \quad (5)$$

In formula (5) the signs $(+)$ and $(-)$ correspond to the length and velocity forms, square of the Bohr radius $a_0^2 = 28.0028$ Mb converts the atomic units for cross-sections to Mb $= 10^{-22}$ m^2, ω is the exciting photon energy in atomic units, and $|\langle \varepsilon\ell j||D||J_0\rangle|$ is the submatrix element of a transition consisting of the sum of the partial amplitudes in accord with scheme (2).

Another physical quantity describing the interaction of unpolarized atoms with linearly polarized ionizing radiation is the parameter of the angular distribution of photoelectrons β defined as follows [22]:

$$\left(\frac{\mathrm{d}\sigma_{J_0}}{\mathrm{d}\Omega}\right) = \frac{\sigma_{J_0}}{4\pi}\left[1 + \beta_{J_0}P_2(\cos\theta)\right]. \quad (6)$$

The expression for β [19] can be also simplified because of the spherical symmetry of the ionic core in the case under consideration and has the form:

see equation (7) below.

In formulae (5, 7) the relativistically corrected continuum wave functions have the following asymptotic form

$$P_{\varepsilon\ell}(r) \underset{r\to\infty}{\longrightarrow} \sqrt{\frac{2}{\pi k}}\sin\left(kr - \frac{\ell\pi}{2} + \frac{Z_{\mathrm{eff}}}{k}\ln(2kr) + \delta_\ell\right). \quad (8)$$

$$\beta_{J_0}(\omega) = \frac{4}{3}\pi^2\alpha a_0^2\omega^{\pm 1}\frac{1}{(2J_0+1)\sigma_{J_0}(\omega)}\sum_{\ell j\ell' j'}(-1)^{j+j'+3/2-J_0}\left[30(2\ell+1)(2\ell'+1)(2j+1)(2j'+1)\right]^{1/2}\mathrm{e}^{\mathrm{i}(\delta_\ell-\delta_{\ell'})} \times \begin{pmatrix} \ell & \ell' & 2 \\ 0 & 0 & 0 \end{pmatrix}\begin{Bmatrix} j' & j & 2 \\ \ell & \ell' & 1/2 \end{Bmatrix}\begin{Bmatrix} 1 & 1 & 2 \\ j' & j & J_0 \end{Bmatrix}\langle \varepsilon\ell j||D||J_0\rangle\langle \varepsilon\ell' j'||D||J_0\rangle^* \quad (7)$$

Here $k^2 = 2\varepsilon(1+\alpha^2\varepsilon/2)$, ε is the photoelectron energy in a.u., $Z_{\rm eff} = Z_{\rm as}(1+\alpha^2\varepsilon)$ with $Z_{\rm as}$ = asymptotic charge of ion (here $Z_{\rm as} = 1$) and the phase shift δ_ℓ represents the sum

$$\delta_\ell = \arg\Gamma\left(\ell + 1 - {\rm i}\frac{Z_{\rm eff}}{k}\right) + \varphi_\ell \qquad (9)$$

where φ_ℓ is the short-range phase shift.

Experiments using polarized excited atoms allow one to determine in addition the ratio of the reduced matrix elements [23–25] which is connected with the partial cross-sections $\sigma^{\ell j}_{J_0}(\omega)$ *via* the formula:

$$\nu^2 \cong \left|\frac{D_{\ell_0+1}}{D_{\ell_0-1}}\right|^2 = \left[\frac{\sum_j \sigma^{(\ell_0+1)j}_{J_0}(\omega)}{\sum_j \sigma^{(\ell_0-1)j}_{J_0}(\omega)}\right] = \left|\frac{\langle\ell_0+1||C^{(1)}||\ell_0\rangle\langle\varepsilon(\ell_0+1)|d|n_0\ell_0\rangle}{\langle\ell_0-1||C^{(1)}||\ell_0\rangle\langle\varepsilon(\ell_0-1)|d|n_0\ell_0\rangle}\right|^2, \qquad (10)$$

as well as the phase shift difference $\Delta(\varepsilon) \equiv \delta_{\ell_0+1}(\varepsilon) - \delta_{\ell_0-1}(\varepsilon)$. In the figures we shall present the quantity $\nu(\varepsilon) = |D_{\rm d}(\varepsilon)/D_{\rm s}(\varepsilon)|$ and $\Delta(\varepsilon)$. We note that the calculated ratios of the radial integrals $\langle\varepsilon d|d|np\rangle\,/\langle\varepsilon s|d|np\rangle$ involved in the reduced matrix elements have negative signs for all the considered alkali atoms Ak(np) near threshold.

2.2 Atomic orbitals

In computing the atomic orbitals (AOs) entering the matrix elements in equations (2–5) we accounted for relativistic and many-electron effects. To take into account relativistic effects we used the Pauli-Fock approximation [19,20] which is known to be sufficient to describe the influence of the relativistic compression of the atomic core on the position of the Cooper minimum in photoionization of ground state alkali atoms with an accuracy of some hundredth of an eV even for heavy atoms, *e.g.* in the 6s-cross-section of Cs [4]. In the Pauli-Fock approach the mass-velocity $H^{\rm m}_{n\ell}$ and Darwin $H^{\rm D}_{n\ell}$ terms are included in the self-consistent solution of the Hartree-Fock equations. These terms have spherical symmetry and therefore do not change the usual nonrelativistic configuration, however, allowing one to take into account the relativistic compression of the atomic core which is found to be considerable for the atoms with $Z \geq 36$ [2,20]. The following term describing the spin-orbit interaction was included in computing the AOs for the optical np-electron:

$$H^{\rm SO}_{n\ell j}(r) = \frac{\alpha^2}{2}\frac{j(j+1) - \ell(\ell+1) - s(s+1)}{2} \times \left[1 + \frac{\alpha^2}{2}(\varepsilon_{n\ell} - V_{n\ell}(r))\right]^{-1}\frac{1}{r}\frac{{\rm d}V_{n\ell}(r)}{{\rm d}r} \qquad (11)$$

where all energies are measured in Rydberg units; $\alpha = 1/137.036$ is the fine structure constant and $V_{n\ell}(r)$ denotes the local part of the Hartree-Fock (HF) potential. In the calculation of $V_{n\ell}(r)$ it is sufficient to use only the monopole terms in the Coulombic expansion (contribution of other terms was found to be 0.5% for Xe).

The influence of many-electron effects on the AOs of the np-optical electron and the $\varepsilon\ell$-photoelectron waves was taken into account by including the core polarization potential $V^{\rm c}_{n\ell}(r)$ (CP) in the PF equation [4]. The CP approach corresponds to the first step of a large scale multi-configurational calculation or, in other words, accounts for the influence of the high-lying configurations on the single-electron PF AOs. The AOs for the optical electron were obtained *via* solution of the following equation:

$$\left(-\frac{{\rm d}^2}{{\rm d}r^2} + \frac{\ell(\ell+1)}{r^2} + V_{n\ell}(r) - X_{n\ell}(r) + H^{\rm m}_{n\ell}(r) + H^{\rm D}_{n\ell}(r) + H^{\rm SO}_{n\ell j}(r) + V^{\rm c}_{n\ell}(r)\right)P_{n\ell j}(r) = \varepsilon_{n\ell j}(r)P_{n\ell j}(r) \qquad (12)$$

where the $V_{n\ell}(r)$ and $X_{n\ell}(r)$ are the local and nonlocal Hartree-Fock potentials and $H^{\rm m}_{n\ell}(r)$, $H^{\rm D}_{n\ell}(r)$, $H^{\rm SO}_{n\ell j}(r)$ are the relativistic corrections mentioned above. The expression for computing the core polarization potential $V^{\rm c}_{n\ell}(r)$ has been derived in [4] applying the variational principle for the total energy of an atom written with the second order correlational corrections. As a result an expression for the product $V^{\rm c}_{n\ell}(r) \otimes P_{n\ell}(r)$ was obtained [4]. To have the possibility to compare our core polarization potential with the potentials used in earlier work [5,6,8,10,11] we construct the local form of this potential $V^{\rm CP}_{n\ell}(r)$ by simply dividing the product $V^{\rm c}_{n\ell}(r) \otimes P_{n\ell}(r)$ by the AO $P_{n\ell}(r)$:

$$V^{\rm CP}_{n\ell}(r) = \frac{V^{\rm c}_{n\ell}(r) \otimes P_{n\ell}(r)}{P_{n\ell}(r)}\,. \qquad (13)$$

The potential $V^{\rm CP}_{n\ell}(r)$ is almost independent of the principal quantum number n. Moreover, the n independent potential $V^{\rm CP}_{\ell}(r)$ can be used for the calculation of the continuum AOs because singularities of $V^{\rm CP}_{n\ell}(r)$ associated with the nodes of $P_{n\ell}(r)$ are not critical for the computation of $P_{n\ell}(r)$ in view of the fact that the nodes in $P_{n\ell}(r)$ and in $V^{\rm c}_{n\ell}(r) \otimes P_{n\ell}(r)$ appear at essentially the same distance r [4]. To compute the potentials $V^{\rm CP}_{\ell}(r)$ we used the AOs of the s-, p-, d-, f-, g-, and h-channels. Each channel contained the AOs of discrete states with a mean radius smaller or equal to 50 a.u. and AOs of continuum states with energies from $0.001Ry$ to $100Ry$. The potentials $V^{\rm CP}_{\ell}(r)$ for the s-, p-, and d-channels are listed in Figure 1 together with the AOs used in equation (10). The core polarization potentials allow us to compute the theoretical corrections $\Delta IP(np)_{\rm TH}$ for the PF ionization potentials of np-electrons $IP(np)_{\rm PF}$ using the formula:

$$\Delta IP(np)_{\rm TH} = \int_0^\infty P_{np}(r)V^{\rm c}_p(r) \otimes P_{np}(r){\rm d}r. \qquad (14)$$

The corrections computed *via* equation (14) are documented in Table 1 together with the full theoretical value

Table 1. Ionization potentials IP [eV] of the optical np-electron and relative difference $\delta\sigma_{\rm LV}$ between the cross-sections, calculated in length ($\sigma_{\rm L}$) and velocity ($\sigma_{\rm V}$) gauge.

	$Na^{(a)}$	$K^{(b)}$	$Rb^{(c)}$	$Cs^{(c)}$
$IP(np_{1/2})_{\rm EXP}$	3.03682	2.73073	2.61641	2.50707
$IP(np_{3/2})_{\rm EXP}$	3.03469	2.72358	2.58695	2.43837
$IP(np)^{(d)}_{\rm EXP}$	3.03539	2.72596	2.59676	2.46127
$IP(np)_{\rm TH}$	3.044	2.733	2.605	2.482
$\Delta IP(np)^{(e)}_{\rm TH}$	0.066	0.132	0.148	0.185
$\delta\sigma_{\rm LV}[\%]^{(f)}$, PF	+2	+25	+27	+25
$\delta\sigma_{\rm LV}[\%]^{(f)}$, CIPF	−2	+10	+10	+5
$\delta\sigma_{\rm LV}[\%]^{(f)}$, CIPFCP	−5	+4	+3	−3

[(a)]Data from [51]. [(b)]Data from [52]. [(c)]Data from [53]. [(d)]Averaged over $IP(np_{3/2})$ and $IP(np_{1/2})$. [(e)]$\Delta IP(np)_{\rm TH} = IP(np)_{\rm TH} - IP(np)_{\rm PF}$. [(f)]Values $\delta\sigma_{\rm LV} = 2(\sigma_{\rm L} - \sigma_{\rm V})/(\sigma_{\rm L} + \sigma_{\rm V})$ are calculated at the photoelectron energy $\varepsilon = 4$ eV.

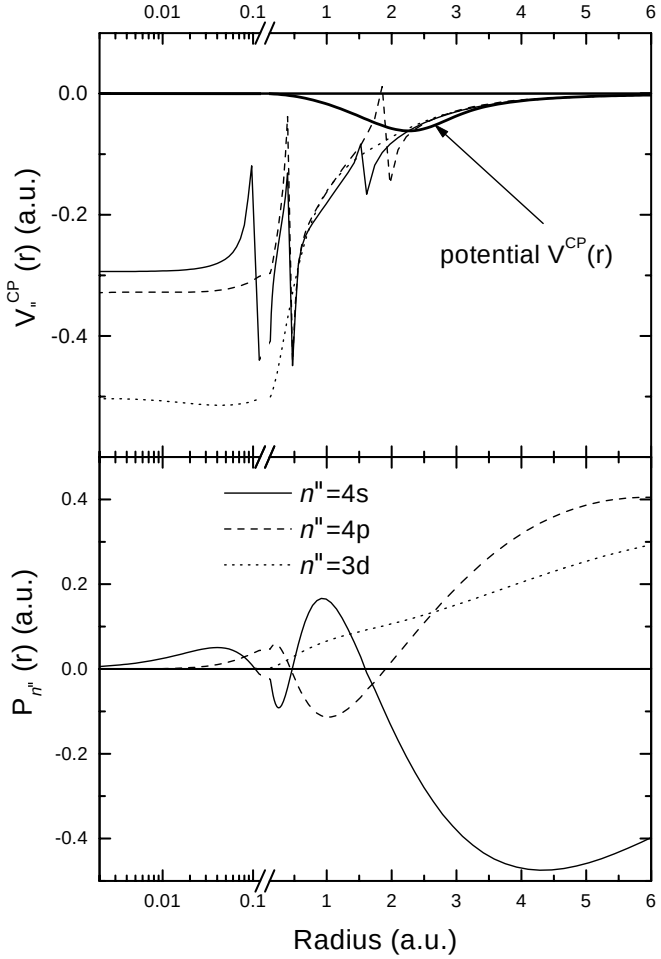

Fig. 1. ℓ-dependent core polarization potentials $V_\ell^{\rm CP}(r)$, equation (13), and atomic orbitals $P_{n\ell}(r)$ used for the "localization" procedure. Thick solid line represents the core polarization potential $V^{\rm CP}(r)$, equation (15).

for the ionization potential $IP(np)_{\rm TH} = IP(np)_{\rm PF} + \Delta IP(np)_{\rm TH}$ and experimental values of $IP(np)_{\rm EXP}$ averaged over the fine structure components of the np-electron. With inclusion of correction (14) the calculated values $IP(np)_{\rm TH}$ agree with the measured ones to within about 20 meV. The values of $\Delta IP(np)_{\rm TH}$ and $IP(np)_{\rm TH}$ listed in Table 1 differ somewhat from the results of paper [4]. The reason for this difference is connected with the fact that in the present work we used the selfconsistent core AOs obtained in the $(n-1)p^6np$ configurations whereas in paper [4] the $(n-1)p^6ns$ configurations were used.

In Figure 1 we also show the potential for the potassium atom which represents the main part of the semiempirical core polarization potential used in papers [5,6,8,10,11]. This potential has the form:

$$V^{\rm CP}(r) = -\frac{\alpha_{\rm d}}{2r^4}\left(1 - \exp\left[-(r/r_{\rm c}^6\right]\right), \qquad (15)$$

where the $\alpha_{\rm d} = 6.07$ a.u. and $r_{\rm c} = 2.36$ a.u. are the dipole polarizability of the ionic core and cut-off radius. The value of $\alpha_{\rm d}$ was obtained by us using the asymptotic behaviour of the potential (15) [4] and the value of $r_{\rm c}$ is chosen such that potential (15) produces the correction $\Delta IP(np)_{\rm TH} = 0.132$ eV (see Tab. 1). The core polarization potentials (13, 15) differ at small radii: while potential (15) goes to zero for $r/r_{\rm c} \ll 1$, our potential (13) reaches a constant nonzero value at small distances.

2.3 Calculations within different approximations and gauges

In this section we present the results of calculations for the total photoionization cross-sections $\sigma(\varepsilon)$ and for the ratio $\nu(\varepsilon)$ of the reduced matrix elements (10), as performed within the PF, CIPF and CIPFCP approximations for the particularly interesting case of potassium. The PF approximation uses the upper pathway of the scheme (2) only. The CIPF approach uses the PF AOs and all the pathways indicated in scheme (2). The CIPFCP approach is similar to CIPF, but the core polarization potential is taken into account in the computation of AOs in accordance with equation (12).

The results of the calculations are documented in Figure 2 for the length (solid lines) and velocity gauges (dashed lines). The PF cross-sections $\sigma_{\rm L}$(PF) and $\sigma_{\rm V}$(PF)

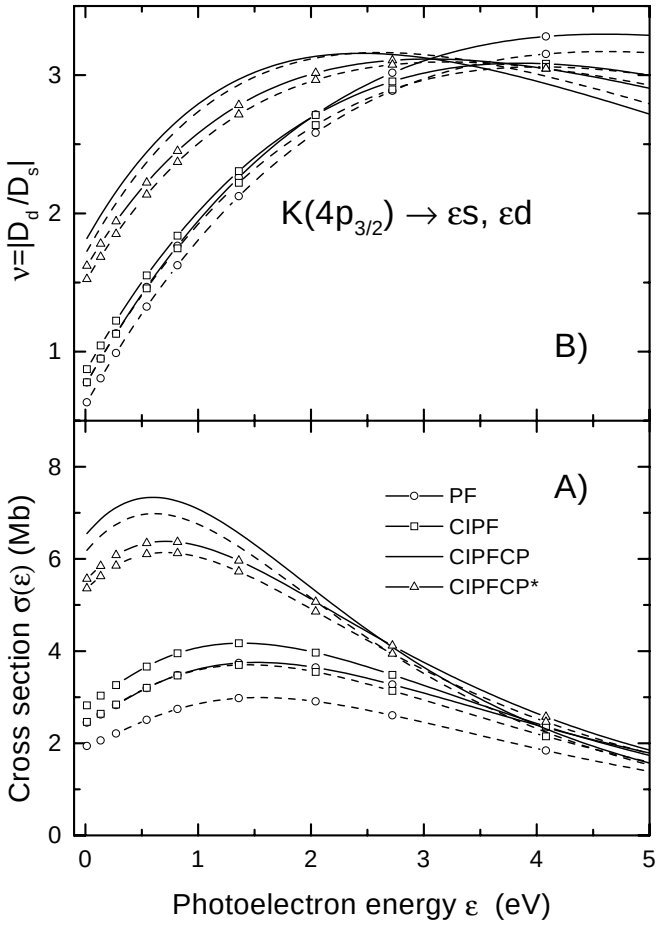

Fig. 2. (A) Photoionization cross-sections σ and (B) ratios ν of the reduced matrix elements, calculated for the K($4p_{3/2}$) atom in different approximations. PF, CIPF and CIPFCP tag the Pauli-Fock, configuration interaction Pauli-Fock and configuration interaction Pauli-Fock with core polarization potential approximations, respectively. CIPFCP* tags the approximation where the CP potential of the form (15) has been used. Solid and dashed lines represent the length and velocity gauge results, respectively.

differ in length and velocity gauges considerably, *e.g.* the relative difference $\delta\sigma_{\rm LV} = 2(\sigma_{\rm L} - \sigma_{\rm V})/(\sigma_{\rm L} + \sigma_{\rm V})$ between $\sigma_{\rm L}$(PF) and $\sigma_{\rm V}$(PF) amounts to 25% at $\varepsilon = 4$ eV. When intershell correlations are taken into account according to scheme (2) (CIPF) the relative difference $\delta\sigma_{\rm LV}$ is reduced to 10% and the cross-sections increase slightly. The inclusion of the core polarization potential (CIPFCP) has a remarkably strong effect on σ and ν for K($4p$) atoms: the near-threshold cross-sections increase by a factor of two. This rise is connected with the d-partial channel and due to the strong sensitivity of the d-AOs on the potential (see also Sect. 4.3). As a result the ratio of the reduced matrix elements ν also increases strongly when core polarization is included. Within CIPFCP the difference $\delta\sigma_{\rm LV}$ goes down to 4%. For clarity in subsequent figures, we present our theoretical results in one gauge only, namely in the velocity gauge. In Table 1 we summarize the relative differences $\delta\sigma_{\rm LV}$ between the cross-sections in length and velocity gauges for all alkali atoms, as obtained at $\varepsilon = 4$ eV.

In Figure 2 we have also included cross-sections σ and ratios ν calculated with use of the semiempirical core polarization potential (15) labelled CIPFCP*. These curves lie somewhat lower than those calculated in the CIPFCP approximation. This finding stems from the different behavior of the potentials (13, 15) at small radii.

3 Photoionization experiment for K($4p_{3/2}$)

In connection with the development of a new, intense laser photoelectron source, based on the CW laser photoionization of excited potassium atoms [13,14], we have carried out experimental studies of the polarization-dependent photoionization cross-section and of the electron angular distributions for laser-excited K($4p_{3/2}$) atoms in the threshold region. In this paper we report results obtained at three selected photoelectron energies, namely $\varepsilon = 0.013$, 0.214, and 0.808 eV. The underlying experiments will be briefly described in this section; details can be found in [14] and will be published in a future paper.

A well-collimated beam of ground state K($4s$) atoms, emerging from a differentially-pumped, resistively-heated stainless steel oven, is excited on the potassium D2 line K($4s$, $F = 2 \rightarrow 4p_{3/2}$, $F = 3$) by an actively stabilized, weak single mode laser (767 nm) in a magnetically-shielded region. Alternatively, we have also used a more efficient excitation scheme by simultaneously pumping the two K($4s$, $F = 1 \rightarrow 4p_{3/2}$, $F = 2$) and K($4s$, $F = 2 \rightarrow 4p_{3/2}$, $F = 3$) hyperfine transitions with a quasi-two-frequency laser, which is also long-term stabilized to the resonance transition; for this purpose the carrier of the EOM generated two-frequency laser is locked to a Doppler-free crossover signal as obtained by saturation spectroscopy in a potassium cell. The excited K($4p_{3/2}$) atoms (density about $10^8/{\rm cm}^3$) are photoionized by a tunable dye laser (Stilbene 3, 455–420 nm, bandwidth about 40 GHz, power typically 100 mW) or by a selected UV line (351 nm) from an Ar ion laser. The alignment in the K($4p_{3/2}$) state is monitored by angle-resolved fluorescence detection [14]. Test measurements (a) with single mode and (b) with two-frequency excitation show that optimal alignment in the K($4p_{3/2}$) state is difficult to reach as a result of (a) hyperfine pumping and (b) the presence of the K($4p_{3/2}$, $F = 2$) state. Relative photoionization cross-sections for K($4p_{3/2}$) atoms have been measured over the photoelectron energy range 0–0.22 eV for parallel and perpendicular linear polarizations of the two lasers under conditions of known alignment of the K($4p_{3/2}$) atoms. The cross-sections increase weakly with rising electron energy [14]. From the polarization dependence of these data and extended measurements at three photoelectron energies (0.027, 0.201, 0.809 eV) we extract the ratio $\nu = |D_{\rm d}/D_{\rm s}|$ of the reduced electric dipole elements $D_{\rm d}$, $D_{\rm s}$ for the d- and s-wave continua and the ratio of the partial d-wave and s-wave cross-sections $\sigma_{\rm d}/\sigma_{\rm s} = |D_{\rm d}/D_{\rm s}|^2$ (see Tab. 2). Absolute cross-sections are determined

Table 2. Characteristics of photoionization of K($4p_{3/2}$) atoms near threshold.

(a) Total cross-section σ.

photoelectron energy [eV]	σ [Mb] experiment	σ [Mb] theory[c]
0.013	6.8(10)[a]	6.2
0.214	7.3(11)[a]	6.7
0.809	7.0(10)[a]	6.9
0.910	7.6(11)[b]	6.8

(b) Ratio $\nu = |D_d/D_s|$ of reduced matrix elements for d-wave and s-wave photoelectron emission.

photoelectron energy [eV]	experiment	theory[c]
0.027	1.92(10)[a]	1.74
0.029	1.70(20)[d]	1.75
0.201	2.22(11)[a]	1.97
0.209	2.07(11)[d]	1.99
0.809	2.75(14)[a]	2.60
0.809	2.64(20)[d]	2.60

(c) Cosine of phase difference $\delta_d - \delta_s$ for photoelectron emission into d- and s-wave.

photoelectron energy [eV]	experiment[d]	QDT[e]	theory[c]
0.029	−0.94(5)	−0.901	−0.978
0.209	−0.86(5)	−0.782	−0.893
0.809	−0.58(5)	−0.543	−0.611

a: Present work (ions); b: [32]; c: present work (CIPFCP); d: present work (photoelectron angular distribution); e: present work, using quantum defects given in [54].

at three photoelectron energies (0.013, 0.214, 0.809 eV) on the basis of the following measurements:

(i) determination of the K($4s$) density in the photoionization region (767 nm excitation laser blocked) from the known potassium beam geometry and a measurement of the atom flux with a Langmuir Taylor detector (rhenium ribbon) [14];
(ii) determination of the excited state fraction from measurements of the saturation curve (resonance fluorescence and/or photoionization current *versus* intensity of excitation laser);
(iii) determination of the beam overlap integral using the beam scanning method (see, *e.g.*, [26]);
(iv) absolute measurement of the photon flux of the ionization laser with a calibrated thermopile detector;
(v) absolute measurement of the total photoion or total photoelectron current under conditions, well characterized through measurements (i) to (iv).

The absolute cross-sections reported in Figure 6A correspond to unpolarized K($4p_{3/2}$) atoms ($\eta = 54.7°$). In addition, we have measured photoelectron angular distributions for polarized K($4p_{3/2}$) atoms at three selected energies (0.029, 0.209, 0.809 eV) by detecting a small fraction of the electrons in a space-fixed direction perpendicular to both the atomic beam and the two anticollinear laser beam directions and rotating the two linear polarization directions simultaneously with combinations of computer-controlled half-wave plates and polarizing prisms, while keeping the angle η between the two polarization directions fixed at either $\eta = 0°$ or $\eta = 90°$. Similar photoionization experiments have been previously carried out by our group for laser-excited Ne($3p$, $J = 3$) and Ar($4p$, $J = 3$) atoms and described in detail in references [25,27,28].

The polarization dependent ion data and the electron angular distributions were analyzed on the basis of formulae, given explicitly in [27,28] for photoionization of atoms with total angular momentum $J = 3$, resulting from the coupling of two subsystems i ($i = 1$, 2) which both possess angular momenta $j_i = 3/2$. In the present case $i = 1$ corresponds to the excited $4p$ ($j_1 = 3/2$) electron and $i = 2$ to the nuclear spin of ^{39}K ($j_2 = 3/2$). We assume the nuclear spin to be frozen in the photoionization process (see the corresponding discussion in the literature [29]); moreover, we neglect – as corroborated by the theoretical results – the effects of spin-orbit coupling which could result in a difference between the phase shifts for the $d_{3/2}$ and the $d_{5/2}$ waves. Thus we obtain simplified formulae [25,27,28] which only contain the relevant two reduced matrix elements D_s and D_d, the phase shift difference $\delta_d - \delta_s$ and – as an experimental parameter – the effective quadrupole alignment of the $4p_{3/2}$ electron. The alignment was determined from the angular distribution of the resonance fluorescence using formulae given in [29]. For the analysis of the ion data we used equations (18, 19) from [27]. The electron angular distributions were analysed on the basis of formulae (6a, 6b) in [28] in conjunction with equations (A10a–A10e) in [28]. We note a printing error in (A10a) where the third term should read $+(1/\sqrt{2})\nu\cos\Delta$. We also mention that the sign of the ratio ν in [28] (due to the use of the pseudo-standard phase convention in [28] for which the ratio $\langle d||C^1||p\rangle \,/\langle s||C^1||p\rangle$ is negative) is defined to be opposite to the sign of our ratios ν (which are negative near

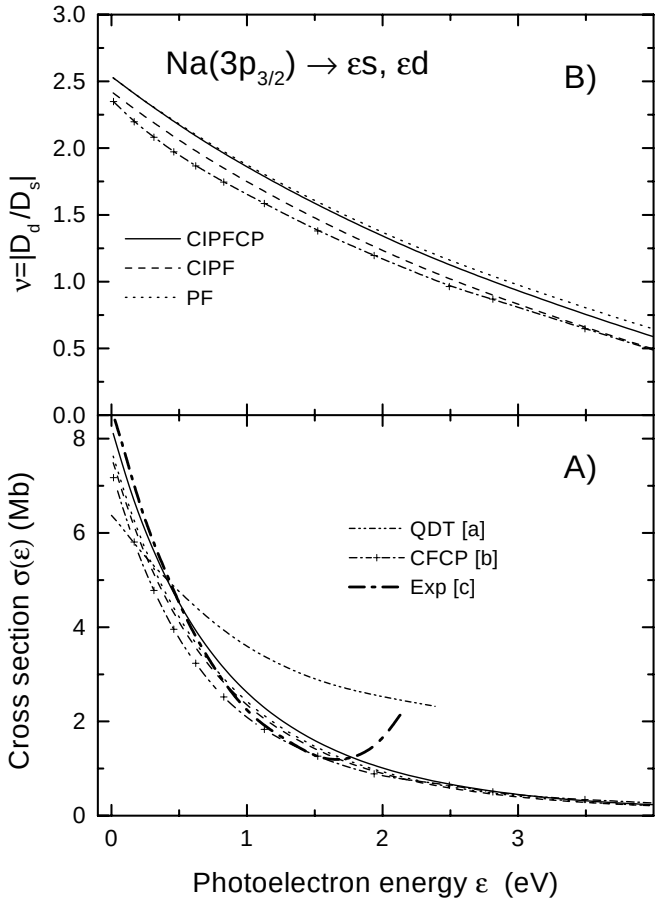

Fig. 3. (A) Photoionization cross-sections σ and (B) ratios ν of the reduced matrix elements for the Na($3p_{3/2}$) atom over the photoelectron energy range 0–4 eV. PF, CIPF, and CIPCP: present calculations (velocity gauge); [a]: quantum defect theory [30]; [b]: central field calculation with core polarization potential [8]; [c]: laser-atomic beam experiment, uncertainty of absolute scale ±25% [15].

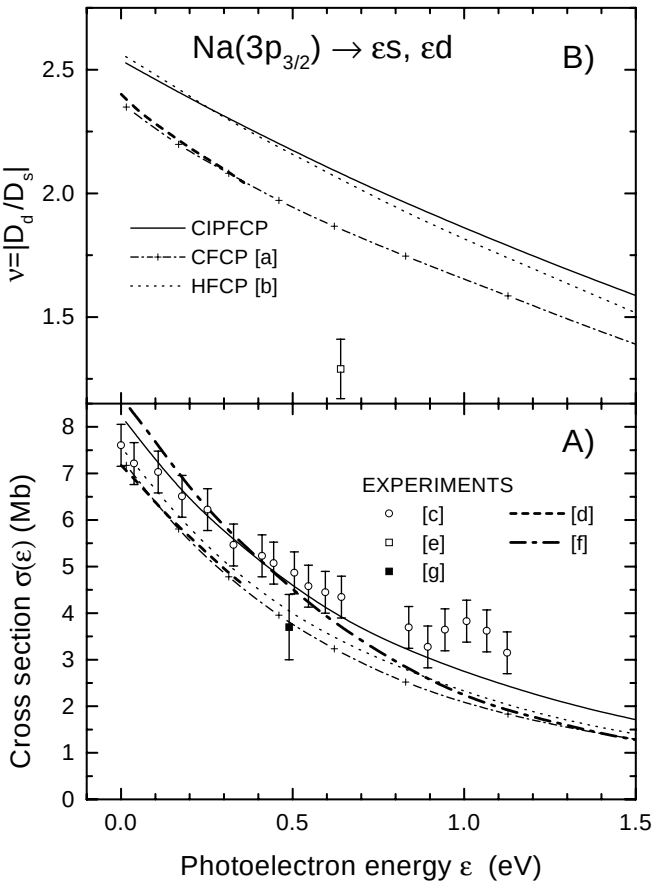

Fig. 4. (A) Photoionization cross-sections σ and (B) ratios ν of the reduced matrix elements for the Na($3p_{3/2}$) atom over the photoelectron energy range 0–1.5 eV. Our theoretical results, computed in the CIPFCP approximation (velocity gauge), are compared with other calculations and measurements. [a]: central field calculation with core polarization potential [8]; [b]: Hartree-Fock calculation with core polarization potential [10]; [c]: cross-sections from electron-ion recombination data [31]; [d]: laser ionization experiment [23], absolute scale adjusted to theoretical cross-sections of Aymar *et al.* [8]; [e]: pulsed laser ionization experiment [24]; [f]: ionization with monochromatized synchrotron radiation, uncertainty of absolute scale ±25%; [g]: saturated ionization with pulsed laser [32].

threshold). This aspect is taken into account in the comparison of our theoretical ratios $\cos(\delta_\mathrm{d}-\delta_\mathrm{s})$ with the values derived from the experiments (which yield the sign of the product $\nu\cos(\delta_\mathrm{d}-\delta_\mathrm{s})$).

4 Results and discussion

4.1 Photoionization of Na($3p_{3/2}$) atoms

In Figures 3 and 4 we present the results for photoionization of Na($3p_{3/2}$) atoms over the photoelectron energy range $\varepsilon = 0{-}4$ eV and $\varepsilon = 0{-}1.5$ eV, respectively. In good agreement with previous calculations (central field with core polarization CFCP [8] and Hartree-Fock with core polarization HFCP [10]) our total calculated cross-sections (Figs. 3A and 4A) are found to drop rapidly with rising energy. The early quantum defect theory calculation [30] produces cross-sections of about the right size, but the energy dependence is too weak. The effects of configuration interaction and core polarization are found to be small for photoionization of Na($3p$). The different approximations PF, CIPF and CIPFCP yield cross-sections (as shown in Fig. 3A for the velocity gauge) which differ by no more than about 10% in absolute size. Weak destructive interference between direct photoionization (upper pathway in (2)) and photoionization through the inner $2p$-shell (lower FISCI channel in (2)) is observed; for the other alkali atoms this interference is a constructive one. The behaviour of the cross-sections in the sodium atom is connected with a relatively strong delocalization of the d-wave at small energies which "covers" both the $2p$- and the $3p$-AOs. The d-partial wave contributes the dominant part to the cross-section near threshold but with rising energy the first node moves into the range of the $3p$-AO, thereby decreasing the respective matrix element; at $\varepsilon = 2.8$ eV

the cross-sections connected with s- and d-partial waves become equal (Fig. 3B).

Energy dependent experimental cross-sections were first derived from electron-ion recombination data by Rothe [31]; they are in rather good agreement with the CIPFCP calculations. Later, Preses *et al.* [15] used a CW multimode dye laser for $3s{-}3p_{3/2}$ excitation and monochromatized synchrotron radiation for ionizing Na($3p_{3/2}$) over the range $\varepsilon = 0{-}2.1$ eV. The absolute scale of the experimental cross-sections was established in a different measurement, using two pulsed lasers (pulse lengths of about 7 ns each) [15]; the authors estimate an uncertainty of $\pm 25\%$ for the size of the cross-section near threshold. The effects of a possible initial state polarization were not discussed for either experiment. We note that the energy dependence of the cross-sections measured in [15] is somewhat steeper than that shown by the calculations in the range $\varepsilon = 0{-}1$ eV; at energies $\varepsilon > 1.6$ eV the experimental cross-section rises again (Fig. 3A) in contrast to the trend shown by all the calculations. Possibly the measurements were influenced by an unnoticed systematic error at the shortest wavelengths ($<$ 240 nm). In later work [32] the same group determined an absolute cross-section of 3.7(7) Mb at the photoelectron energy $\varepsilon = 0.47$ eV (solid square with error bar in Fig. 4A); this value was obtained with a saturation method which does not require knowledge of the atom density. Effects of initial state polarization were found to be below 5% by varying the angle between the polarization directions of the two linearly-polarized pulsed lasers. The earlier result 4.8(12) Mb at $\varepsilon = 0.47$ eV [15] agrees with the latter [32] within the experimental errors. The comparison between theory and experiment in Figure 4A shows that the experimental uncertainties in the absolute cross-sections have to be reduced further to allow a critical test of the different theoretical results.

In Figures 3B and 4B we present the ratio $\nu = |D_\mathrm{d}/D_\mathrm{s}|$ of the reduced electric dipole elements D_d and D_s for electron emission into the d-wave and s-wave. For electron energies below about 3 eV the d-wave cross-section $\sigma_\mathrm{d} = D_\mathrm{d}^2$ is larger than that for s-wave emission $\sigma_\mathrm{s} = D_\mathrm{s}^2$. Two groups have studied the ratio ν experimentally. Duong *et al.* [23] used anticollinear lasers to excite Na($3s$, $F = 2$) atoms to the Na($3p_{3/2}$, $F = 3$) state with a stabilized, circularly-polarized single frequency laser and to ionize the excited atoms with pulsed coherent UV light, obtained by frequency doubling of a laser-pumped, temperature tunable parametric oscillator. The UV light was also circularly polarized, and the sense of rotation was chosen identical with or opposite to that of the exciting laser. A guiding magnetic field of a few tenths mT along the propagation directions of the lasers was applied. Photoions were extracted by a weak electric field (2 V/cm) and detected with an electron multiplier. From the ion count rates, measured for parallel (S_+) and antiparallel (S_-) circular polarizations, the ratio $\rho = S_+/S_- = 6\sigma_\mathrm{d}/(\sigma_\mathrm{d} + 10\sigma_\mathrm{s})$ and therefrom the ratio $\sigma_\mathrm{d}/\sigma_\mathrm{s} = \nu^2 = D_\mathrm{d}^2/D_\mathrm{s}^2$ was obtained over the range $\varepsilon = 0{-}0.5$ eV (see also discussion in Sect. 4.3 for similar experiments on Rb($5p_{3/2}$)). The results of Duong *et al.* [23] are in good agreement with the theoretical values of Aymar *et al.* [8], but are lower than our CIPFCP data and the results of Laughlin [10] computed in HF approximation with inclusion of core polarization (HFCP) (Fig. 4B). The open circle at $\varepsilon = 0.64$ eV is due to Hansen *et al.* [24] who used two pulsed lasers (a dye laser with 4 ns FWHM for $3s{-}3p_{3/2}$ excitation and a nitrogen laser (337 nm) with 7–10 ns FWHM for ionization) and detected the photoelectrons in an angular-resolved way for several angles η between the electric vectors of the two linearly-polarized lasers. In their data evaluation they took the effects of the coherently excited hyperfine structure on the time evolution of the excited state into account. Their ratio $\nu = 1.29(12)$ is significantly lower than all the calculated values and the value extrapolated from the results of Duong *et al.* [23]; it is likely that the low ν value of Hansen *et al.* [24] reflects a systematic error, possibly associated with the nontrivial influence of the hyperfine structure. From their angular distributions, Hansen *et al.* [24] also extracted the quantity $\cos(\delta_\mathrm{d} - \delta_\mathrm{s})$ where $\delta_\mathrm{d} - \delta_\mathrm{s}$ is the difference between the phase shifts of the two final electron continuum waves (we note that the effect of spin-orbit coupling which results in a difference between the phase shifts for the $d_{3/2}$ and the $d_{5/2}$ waves is negligible, therefore in Figure 5 (left side) we document the results for the phase shifts averaged over the total angular momentum of d-electron). Their result $\cos(\delta_\mathrm{d} - \delta_\mathrm{s}) = 0.81(9)$ is a little below our theoretical result $\cos(\delta_\mathrm{d} - \delta_\mathrm{s}) = 0.918$. We note that an estimate of $\cos(\delta_\mathrm{d} - \delta_\mathrm{s})$, based on the quantum defect theory expression for the phase shift $\delta_\ell = \arg\Gamma(\ell+1-\mathrm{i}/k)+\pi\mu_\ell$, yields the result 0.92 at $\varepsilon = 0.64$ eV in close agreement with our calculation; here, k is the electron momentum in atomic units and μ_ℓ represents the extrapolated quantum defect.

In Figure 5 we present the energy dependence of the phase difference $\Delta = \delta_\mathrm{d} - \delta_\mathrm{s}$ (left side) and of the angular distribution parameter β which describes the photoelectron angular distribution involving unpolarized excited Ak($np_{3/2}$) atoms. Note that the phase difference calculated within the PF and the CIPF approximation are identical because of the absence of an imaginary part in the transition amplitude (2) in the considered photoelectron energy range. In Figure 5 we show the phase differences calculated within the CIPF approximation. To our knowledge, experimental results for the quantity $\cos(\delta_\mathrm{d} - \delta_\mathrm{s})$ are only available for Ak = Na (see above) and K (see discussion in Sect. 4.2). For Na($3p$) the CIPF and CIPFCP phase differences are nearly identical, and the β-values, calculated in the three approximations, only differ significantly for $\varepsilon > 2$ eV. For the heavier alkali atoms the energy dependences of both Δ and β exhibit similar trends (monotonous rise with energy). The results for K($4p$) appear to be most sensitive to the approximation used (see also Sects. 2.3 and 4.2).

4.2 Photoionization of K(4p) atoms

In contrast to the situation for Na($3p$), the theoretical results obtained for K($4p$) in the different approximations

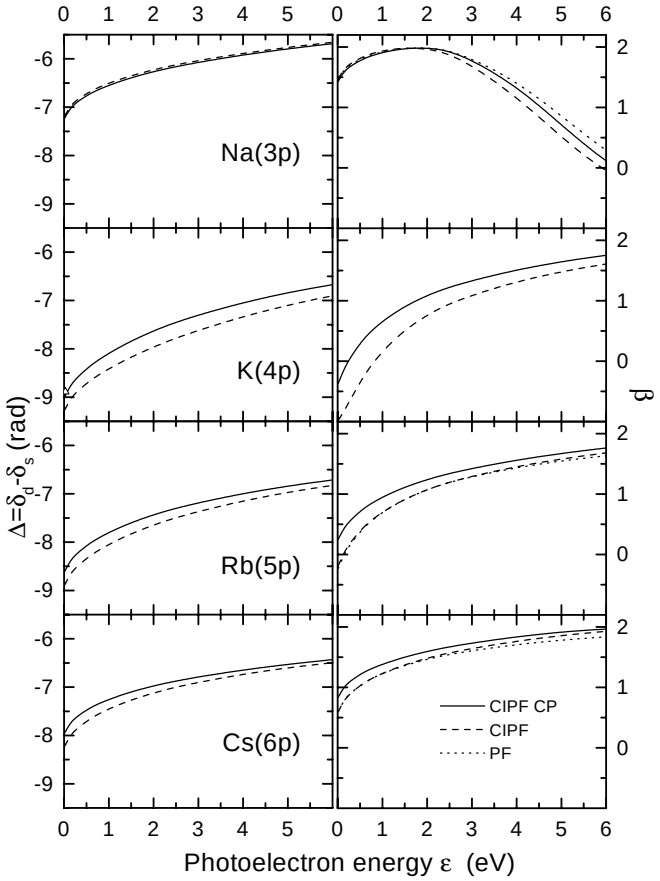

Fig. 5. Phase difference $\Delta = \delta_{\rm d} - \delta_{\rm s}$ (left side) and electron angular distribution parameter β, calculated in different approximations for excited alkali atoms.

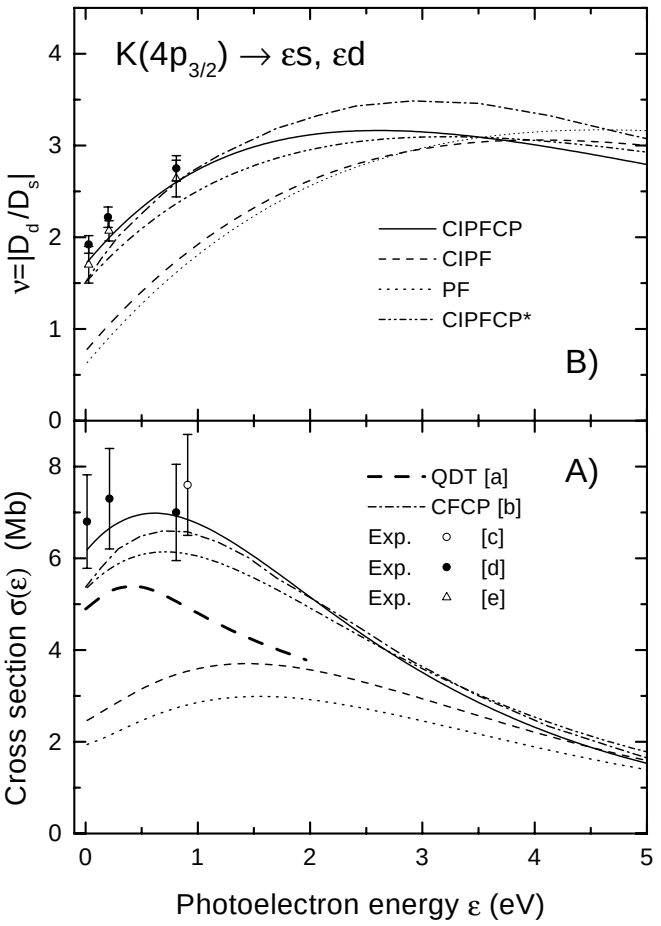

Fig. 6. (A) Photoionization cross-sections σ and (B) ratios ν of the reduced matrix elements for the K($4p_{3/2}$) atom over the photoelectron energy range 0–5 eV. PF, CIPF, CIPFCP, CIPFCP*: present calculations (velocity gauge), see text; [a]: quantum defect theory [30]; [b]: central field calculation with core polarization potential [8]; [c]: saturated ionization with pulsed laser [32]; [d]: CW laser ionization, ion data (present work); [e]: CW laser ionization, photoelectron angular distribution data (present work).

(PF, CIPF and CIPFCP), are found to differ substantially (see Fig. 6). The inclusion of core polarization is very important and raises the CIPF cross-section near threshold by more than a factor of two. Therefore photoionization of K($4p$) atoms provides a good test for the quality of theoretical descriptions. In Figure 6A we include results obtained with three different ways to account for core polarization (the central field with core polarization due to Aymar *et al.* [8] (CFCP), our CIPFCP approach and a modified CIPFCP calculation (labelled CIPFCP*) in which a core polarization potential (15) was used as constructed along the lines proposed by Norcross [6]). These three descriptions yield similar shapes of the cross-section; near threshold the respective absolute values differ by less than 20% and are found to be in satisfactory agreement with the most recent experimental measurements. Burkhardt *et al.* [32] used a saturation method and obtained 7.6(11) Mb at $\varepsilon = 0.79$ eV (open circle). Our experimental cross-sections (see Tab. 2), obtained with the procedure outlined in Section 3 and presented for the case of unpolarized K($4p_{3/2}$) atoms in Figure 6A (filled dots), are in very good agreement with the CIPFCP calculations and with the value measured by Burkhardt *et al.* [32]. In Figure 6A we did not include the early experimental results reported by Nygaard *et al.* [33] at four wavelengths in the range 450–250 nm ($\varepsilon = 0.03-1.82$ eV). Near threshold these authors obtained about 5 Mb, a value compatible with our result within the respective error limits; towards higher energies their cross-sections are found to decrease rapidly and reach a value of about 0.3 Mb at 250 nm, which appears far too low. We attribute this behaviour to limitations in signal-to-noise ratio and/or unnoticed systematic errors at shorter wavelengths (see also the discussion of the Cs($6p$) cross-sections due to Nygaard's group [34] below). In conclusion of this subsection we note that the earlier quantum defect theory (QDT) calculation of Moskvin [30] which yielded unexpectively good results for Rb($5p$) and Cs($6p$) (see Figs. 7 and 8), produced cross-sections for K($4p$) which lie above those due to PF and CIPF, but significantly below CIPFCP and the experimental results.

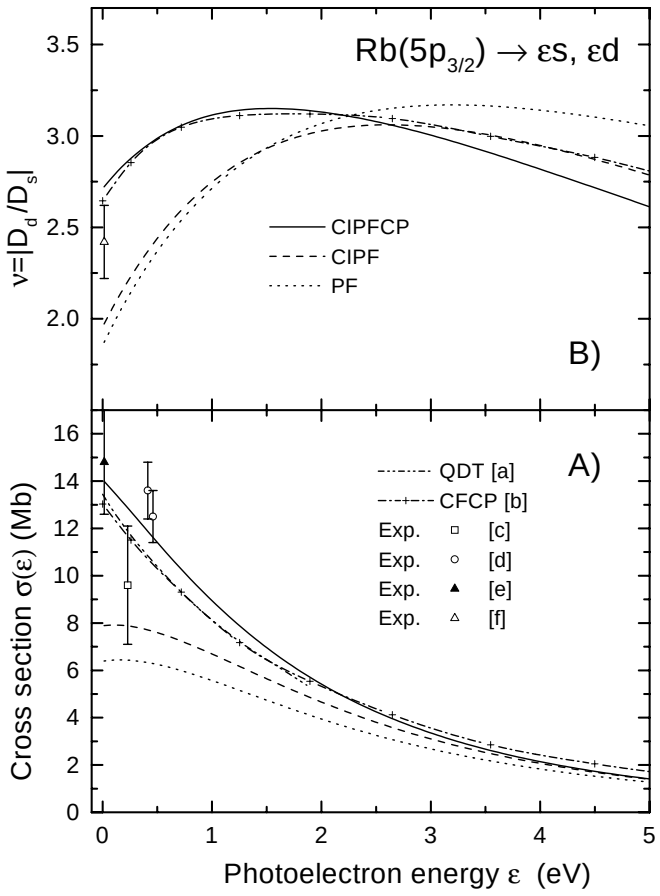

Fig. 7. (A) Photoionization cross-sections σ and (B) ratios ν of the reduced matrix elements for the Rb($5p_{3/2}$) atom over the photoelectron energy range 0–5 eV. PF, CIPF, CIPFCP: present calculations (velocity gauge); [a]: quantum defect theory [30]; [b]: central field calculation with core polarization potential [11]; [c]: laser ionization at 440 nm [36]; [d]: laser ionization of trapped atoms at 413 and 407 nm [37]; [e]: laser ionization of trapped atoms at 476.5 nm [38]; [f]: laser ionization at 476.5 nm using circularly-polarized exciting and ionizing lasers [39,41] (see text for details).

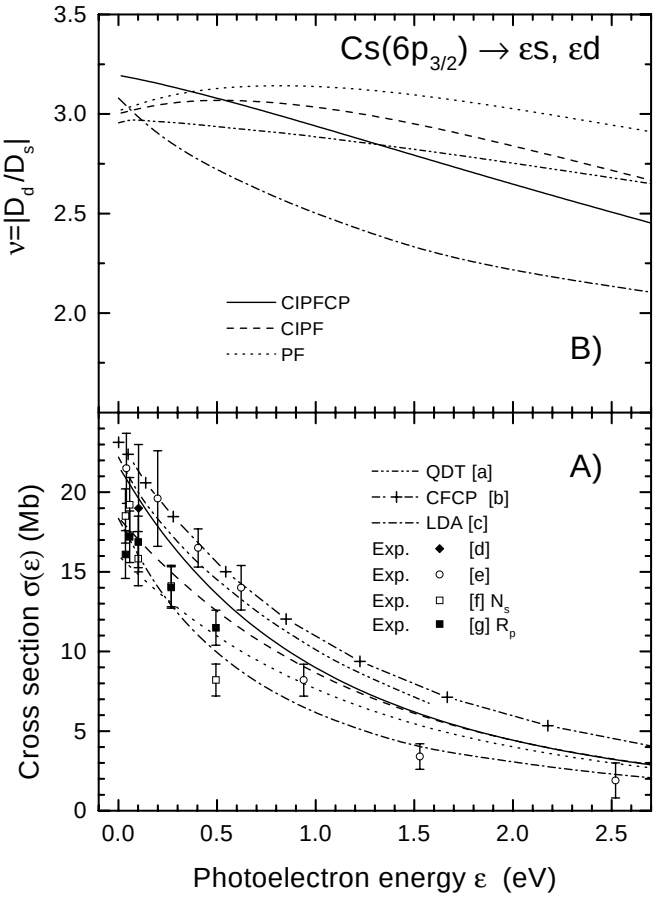

Fig. 8. (A) Photoionization cross-sections σ and (B) ratios ν of the reduced matrix elements for the Cs($6p_{3/2}$) atom over the photoelectron energy range 0–2.7 eV. PF, CIPF, CIPFCP: present calculations (velocity gauge); [a]: quantum defect theory [30]; [b]: central field calculation with core polarization potential [5]; [c]: local density approximation [48]; [d]: laser ionization of a statistical mixture of Cs($6p_{1/2}$) and Cs($6p_{3/2}$) atoms at 488 nm [49]; [e]: ionization with monochromatized Hg–Xe lamp [34]; [f]: laser ionization of trapped atoms; cross-sections derived from number of atoms in trap [50]; [g]: laser ionization of trapped atoms; cross-sections derived from trap loss rate [50].

In Figure 6B we present the ratio ν of the reduced matrix elements. The CIPFCP results are closest to our experimentally derived ratios. We note that the polarization dependent ion data and the electron angular distribution experiments yielded identical results for the ratio ν within the respective uncertainties (Tab. 2). The consistency of the CIPFCP results and the experimental values for both the absolute cross-sections and the ratios ν demonstrates that our approach is capable to account for the effects of core polarization in a realistic way. We attribute the strong influence of core polarization, as mirrored by the large difference between the CIPF and the CIPFCP results, to the fact that for the atomic number $Z = 19$ the collapse of the d-orbital to smaller radial distances starts to occur (see, *e.g.*, [35]); correspondingly a proper description of the bound and free d-electron wave functions requires the inclusion of rather weak interactions beyond those taken into account in the CIPF calculations.

From fits to the electron angular distributions measured at three photoelectron energies we determined the quantity $\cos(\delta_d - \delta_s)$. The results are listed in Table 2 and compared with the CIPFCP results and QDT values. Good agreement is observed with the CIPFCP results.

4.3 Photoionization of Rb($5p_{3/2}$) atoms

In Figure 7A we compare theoretical photoionization cross-sections for unpolarized Rb($5p_{3/2}$) atoms with available experimental data [36–38]. The effect of core polarization is seen to raise the cross-section near threshold by about a factor 1.77 relative to the CIPF results. Good overall agreement is observed between our CIPFCP results and the central field with core polarization (CFCP) calculations of Aymar *et al.* [11], both for the cross-sections

(Fig. 7A) and ν-values (Fig. 7B). Three different types of model potentials were tried in [11], using the dipole operator in length (or modified length) form; the cross-sections near threshold were found to lie between 12.5 and 14.0 Mb. In Figure 7 we present the results of model (iii) in [11] which may be considered the most appropriate. The early semiempirical calculation of Moskvin [30] happens to coincide with the CFCP (iii) results [11].

The first experimental cross-section was reported by Klyucharev and Sepman [36]. They used a HeCd laser (440 nm) to ionize Rb atoms in a vapour cell, excited to the two Rb($5p_{1/2,3/2}$) resonance states with unpolarized light of an unfiltered rubidium resonance lamp. The Rb($5p$) density was determined by an absorption method. Their cross-section 9.6(20) Mb (1σ uncertainty) is somewhat low in comparison with the CIPFCP and CFCP results. More recently, three measurements have been carried out on photoionization of cold, trapped Rb($5p_{3/2}$) atoms [37–39]. In a pioneering experiment, Gould's group [37] demonstrated the virtue of using cold atoms in a magneto-optical trap for quantitative photoionization studies. They determined the loss rate of Rb atoms from the trap in the presence of ionizing light (intensity about 1 W cm^{-2}) at the two wavelengths 413 and 407 nm (Kr ion laser; $\varepsilon = 0.413$ eV and 0.460 eV). From the corresponding photoionization rate, the fractional population of excited Rb($5p_{3/2}$) atoms and the intensity of the ionizing light they determined the cross-sections as 13.6(12) Mb and 12.5(11) Mb, respectively; these values are close to the CIPFCP and CFCP results. We note that this experiment deals with an effectively unpolarized sample of excited atoms Rb($5p_{3/2}$) atoms due to spatially varying polarizations of the trapping laser beams across the photoionization volume [40]; no variation of the angular-resolved fluorescence from the trapped atoms was observed when a linear polarizer was rotated in front of the fluorescence detector [40]. In another experiment on trapped Rb atoms, Gabbanini *et al.* [38] measured a photoionization cross-section of 14.8(22) Mb close to threshold ($\varepsilon = 0.04$ eV) from the change of the filling rate of a magneto-optical trap with and without a photoionizing Ar ion laser (476.5 nm). This value is in good agreement with the CIPFCP and CFCP results. In a subsequent experiment, Gabbanini *et al.* [39] used a time-resolved method to determine the polarization dependence for photoionization of Rb($5p_{3/2}$) atoms, oriented with circularly-polarized light and ionized by (nearly) collinear, circularly-polarized light with the same sense of rotation in the atom frame (signal S_+) and with opposite sense of rotation (signal S_-) as the orienting laser. The trapping and orienting lasers were alternatively switched on and off by acousto-optical modulators for intervals of 1.2 ms and 0.8 ms, respectively. The ionizing laser was switched on for the last 0.4 ms of the orientation phase. Photoions were detected with a channel electron multiplier. From the comparison of the theoretical ratio $\rho \equiv S_+/S_- = 6\nu^2/(\nu^2+10)$ [23,25,39] (valid for complete orientation of the Rb($5p_{3/2}$) atoms and clean circular polarization of the ionizing light) with the experimental ratio $\rho = 2.22 \pm 10\%$ [41] they deduced a ratio of the d-wave to s-wave cross-section $\nu^2 = \sigma_d/\sigma_s = 10\rho/(6-\rho)$ of 5.87(93) [39,41]. This ratio corresponds to a ratio of the respective reduced E1 matrix elements $\nu = |D_d/D_s| = (\sigma_d/\sigma_s)^{1/2}$ of 2.42(20), somewhat below the ratios obtained in the CIPF and CIPFCP calculations (Fig. 7B). The CIPFCP result $\nu = 2.75$ at $\varepsilon = 0.04$ eV corresponds to a ratio $\rho = 2.584$ which is close to the maximum value $\rho = 2.5$ found in the intensity dependent measurements of ρ [39].

4.4 Photoionization of Cs($6p_{3/2}$) atoms

Photoionization of excited Cs($6p$) atoms has been studied for some time. Quite early, experimental work on electron-Cs$^+$ recombination yielded information on the reverse process of photoionization [42–44]. Later, theoretical cross-sections were generated by use of quantum defect theory (QDT) [30,45], followed by central field calculations with inclusion of core polarization [5,46] and by computations within Hartree-Fock [47] and the local density approximation [48]. An absolute experimental value of the photoionization cross-section for a statistical mixture of Cs($6p_{1/2}$) and Cs($6p_{3/2}$) was reported at 488 nm [49]. Subsequently, the wavelength dependence of the cross-section for both Cs($6p$) fine-structure levels was measured by Nygaard *et al.* [34]. They used a filtered Cs resonance lamp for excitation and monochromatized light from a mercury-xenon lamp (wavelength range 500 to 250 nm) for ionization. They normalized their relative cross-sections to the central field calculation with core polarization (CFCP) of Weisheit at 436 nm ($\sigma(6p_{1/2}) = 17.5(18)$ Mb, $\sigma(6p_{3/2}) = 16.5(12)$ Mb [5,34]). More recently, cold Cs atoms in a magneto-optical trap (MOT) were used to study the photoionization of Cs($6p_{3/2}$) from threshold to 423 nm (photoelectron energies 0–0.5 eV) [50]. Cross-sections were obtained in two ways:

(i) the change in the atom loading rate into the trap due to photoionization was observed;
(ii) the steady-state value of the number of trapped atoms as a function of the intensity of the photoionization laser was determined.

In both cases, the intensity of the photoionization laser and the excited state fraction of Cs($6p_{3/2}$) relative to Cs($6s_{1/2}$) have to be known in order to determine the absolute photoionization cross-section.

In Figure 8A we compare previous results for the photoionization cross-section of Cs($6p_{3/2}$) atoms with our theoretical calculations on the Pauli-Fock (PF), configuration interaction Pauli-Fock (CIPF) and the CIPFCP level. We note that the central field calculation with core polarization of Norcross [46] and the Hartree-Fock calculation of Msezane [47] (not shown in Fig. 8A) practically coincide with the CIPFCP and CIPF cross-sections, respectively. To explore the reason for the unexpected coincidence of the HF [47] and the CIPF cross-sections we also carried out a HF calculation which yielded the same result as [47]. We conclude that the decrease of the PF cross-sections

(relative to HF) due to the relativistic compression of the AOs is practically compensated by the constructive interference of the additional CIPF pathways in scheme (2). The CIPFCP and the central field calculation with core polarization of Weisheit [5] agree to within 10% near threshold; the values due to the early QDT calculation (which did not consider the influence of fine-structure) [30] lie in between. The other calculations including the PF and CIPF methods yield somewhat lower cross-sections which actually tend to be in better agreement with the recent experimental MOT results of Marago *et al.* [50]. The significant deviation of the CIPFCP results from the MOT data may indicate that the latter cross-sections are somewhat low on average in view of the fact that the CIPFCP approach has worked very well for the other alkali atoms. To our knowledge no experimental determinations of the ratio $|D_d/D_s|$ (Fig. 8B) have been reported to date.

As for the other alkali atoms, more accurate experimental results of the total and partial photoionization cross-sections for excited Cs($6p$) atoms are needed to provide a stringent test of the theoretical calculations.

5 Concluding remarks

The effect of core polarization, induced by the outer valence/continuum electron, on near-threshold photoionization of excited alkali atoms Ak(np) (Ak = Na–Cs; $n = 3-6$) has been investigated theoretically by comparison of results for the total and partial cross-sections obtained in three different approximations, namely Pauli-Fock (PF), configuration interaction Pauli-Fock (CIPF), and configuration interaction Paul-Fock plus core polarization (CIPFCP) calculations. The core polarization potential has been computed with a novel approach, recently described and applied to ground state alkali atoms and metastable rare gas atoms [4]. While for Na($3p$) CIPF and CIPFCP yield results rather close to those of the single particle PF approximation, the situation is quite different for the heavier alkali atoms K($4p$), Rb($5p$), and Cs($6p$). The effects of configuration interaction (CIPF) raise the cross-sections by about 20% relative to the PF results; even more importantly, core polarization effects are found to strongly increase the cross-sections (mainly in the d-wave channel) by up to a factor of two near threshold. The influence of core polarization is most pronounced for K($4p$) and attributed to the collapse of the d-orbital towards smaller distances which starts to occur for atomic number $Z = 19$ [35] and thereby produces a large sensitivity to comparatively small interactions. The theoretical results are compared with available experimental data, including recent results for cold Rb($5p_{3/2}$) [37–39] and Cs($6p_{3/2}$) atoms [50] in a magneto-optical trap and laser-excited, polarized K($4p_{3/2}$) atoms in a collimated atomic beam [14].

Generally, good agreement is found between the calculations which incorporate core polarization effects and the experimental results. The experimental uncertainties, however, are often too large to allow a sensitive test of the different advanced theoretical approaches. It is desirable to produce experimental benchmark cross-sections with uncertainties below about 5% over extended energy ranges, *e.g.* by using monochromatized synchrotron radiation to photoionize samples of excited Ak(np) atoms with well-characterized density and polarization.

This work has been supported by the Deutsche Forschungsgemeinschaft, by the Stiftung Rheinland-Pfalz für Innovation, by Graduiertenkolleg "Laser-und Teilchenspektroskopie" and by the Zentrum für Lasermesstechnik und Diagnostik. We thank M. Allegrini for providing potassium vapour cells and J. Bömmels, A. Gopalan, M. Reicherts, M.-W. Ruf, J.M. Weber and K. Zinsmeister for experimental and technical support. We acknowledge P.L. Gould and C. Gabbanini for helpful discussions of their work. IDP and VLS gratefully acknowledge the hospitality extended by members of the Fachbereich Physik at the University of Kaiserslautern.

References

1. F.J. Wuilleumier, D.L. Ederer, J.L. Picque, Adv. At. Mol. Phys. **23**, 197 (1988).
2. R. Kau, I.D. Petrov, V.L. Sukhorukov, H. Hotop, J. Phys. B **31**, 1011 (1998).
3. M.G.J. Fink, W.R. Johnson, Phys. Rev. A **34**, 3754 (1986).
4. I.D. Petrov, V.L. Sukhorukov, H. Hotop, J. Phys. B **32**, 973 (1999).
5. J.C. Weisheit, J. Quant. Spectr. Radiat. Transfer **12**, 1241 (1972).
6. D.W. Norcross, Phys. Rev. A **7**, 606 (1973).
7. T.N. Chang, J. Phys. B **8**, 743 (1975).
8. M. Aymar, E. Luc-Koenig, F. Combet Farnoux, J. Phys. B **9**, 1279 (1976).
9. M. Aymar, J. Phys. B **11**, 743 (1978).
10. C. Laughlin, J. Phys. B **11**, 1399 (1978).
11. M. Aymar, O. Robaux, S. Wane, J. Phys. B **17**, 993 (1984).
12. W. Müller, J. Flesch, W. Meyer, J. Chem. Phys. **80**, 3297 (1984).
13. J.M. Weber, E. Leber, M.-W. Ruf, H. Hotop, Phys. Rev. Lett. **82**, 516 (1999).
14. E. Leber, Ph.D. thesis, University Kaiserslautern, 1999 (in preparation).
15. J.M. Preses, C.E. Burkhardt, R.L. Corey, D.L. Earsom, T.L. Daulton, W.P. Garver, J.J. Leventhal, A.Z. Msezane, S.T. Manson, Phys. Rev. A **32**, 1264 (1985).
16. H. Schmoranzer, A. Ehresmann, F. Vollweiler, V.L. Sukhorukov, B.M. Lagutin, I.D. Petrov, K.-H. Schartner, B. Möbus, J. Phys. B **26**, 2795 (1993).
17. V.L. Sukhorukov, B.M. Lagutin, I.D. Petrov, H. Schmoranzer, A. Ehresmann, K.-H. Schartner, J. Phys. B **27**, 241 (1994).
18. B.M. Lagutin, I.D. Petrov, V.L. Sukhorukov, S.B. Whitfield, B. Langer, J. Viefhaus, R. Wehlitz, N. Berrah, W. Mahler, U. Becker, J. Phys. B **29**, 937 (1996).
19. R. Kau, I.D. Petrov, V.L. Sukhorukov, H. Hotop, J. Phys. B **29**, 5673 (1996).
20. R. Kau, I.D. Petrov, V.L. Sukhorukov, H. Hotop, Z. Phys. D **39**, 267 (1997).
21. A.P. Jucis, I.B. Levinson, V.V. Vanagas, *Mathematical apparatus of the Theory of Angular Momentum* (Jerusalem: Israel Program of Scientific Translations, 1962).

22. A. Sommerfeld, G. Schur, Ann. Physik **4**, 409 (1930).
23. H.T. Duong, J. Pinard, J.-L. Vialle, J. Phys. B **11**, 797 (1978).
24. J.C. Hansen, J.A. Duncanson, R.-L. Chien, R.S. Berry, Phys. Rev. A **21**, 222 (1980).
25. A. Siegel, J. Ganz, W. Bussert, H. Hotop, J. Phys. B **16**, 2945 (1983).
26. P. Defrance, F. Brouillard, W. Claeys, G. van Wassenhove, J. Phys. B **14**, 103 (1981).
27. S. Schohl, D. Klar, N.A. Cherepkov, I.D. Petrov, K. Ueda, S. Baier, R. Kau, H. Hotop, J. Phys. B **30**, 609 (1997).
28. S. Schohl, N.A. Cherepkov, I.D. Petrov, V.L. Sukhorukov, S. Baier, H. Hotop, J. Phys. B **31**, 3363 (1998).
29. I.V. Hertel, W. Stoll, Adv. At. Mol. Phys. **13**, 113 (1978).
30. Yu V. Moskvin, Opt. Spectr. **15**, 316 (1963).
31. D.E.J. Rothe, J. Quant. Spectrosc. Radiat. Transfer **9**, 49 (1969).
32. C.E. Burkhardt, J.L. Libbert, Xu. Jian, J.J. Leventhal, J.D. Kelley, Phys. Rev. A **38**, 5949 (1988).
33. K.J. Nygaard, R.J. Corbin, J.D. Jones, Phys. Rev. A **17**, 1543 (1978).
34. K.J. Nygaard, R.E. Hebner Jr, J.D. Jones, R.J. Corbin, Phys. Rev. A **12**, 1440 (1975).
35. R.D. Cowan, *The Theory of Atomic Structure and Spectra* (University California Press, Berkeley, USA, 1981), p. 232.
36. A.N. Klyucharev, V.Yu. Sepman, Opt. Spectrosc. **38**, 712 (1975).
37. T.P. Dinneen, C.D. Wallace, K.-T.N. Tan, P.L. Gould, Optics Lett. **17**, 1706 (1992).
38. C. Gabbanini, S. Gozzini, A. Lucchesini, Opt. Commun. **141**, 25 (1997).
39. C. Gabbanini, F. Ceccherini, S. Gozzini, A. Lucchesini, J. Phys. B **31**, 4143 (1998).
40. P.L. Gould (private communication, 1998).
41. C. Gabbanini (private communication, 1999).
42. F.L. Mohler, C. Boeckner, J. Res. Natl. Bur. Stand. (US) **2**, 489 (1929).
43. F.L. Mohler, J. Res. Natl. Bur. Stand. (US) **10**, 771 (1933).
44. L. Agnew, C. Summers, *Proc. 7th International Conference on the Physics of Ionized Gases* (Belgrade, 1965), p. 574.
45. D.W. Norcross, P.M. Stone, J. Quant. Spectrosc. Radiat. Transfer **6**, 277 (1966).
46. D.W. Norcross, results cited in [34].
47. A.Z. Msezane, J. Phys. B **16**, 489 (1983).
48. J. Lahiri, S.T. Manson, Phys. Rev. A **33**, 3151 (1986).
49. A.N. Klyucharev, B.V. Dobrolege, *Abstracts VIII ICPEAC*, edited by B.C. Cobic, M.V. Kurepa (Belgrade, 1973), p. 553.
50. O. Marago, D. Ciampini, F. Fuso, E. Arimondo, C. Gabbanini, S.T. Manson, Phys. Rev. A **57**, R4110 (1998).
51. W.C. Martin, R. Zalubas, J. Phys. Chem. Ref. Data **10**, 153 (1981).
52. C. Corliss, J. Sugar, J. Phys. Chem. Ref. Data **8**, 1109 (1979).
53. C.E. Moore, *Atomic Energy Levels* (NBS Circular No. 467, Washington, DC: US Govt. Printing Office, 1971).
54. C.-J. Lorenzen, K. Niemax, L.R. Pendrill, Optics Commun. **39**, 370 (1981).